



Deposited via The University of Sheffield.

White Rose Research Online URL for this paper:

<https://eprints.whiterose.ac.uk/id/eprint/149128/>

Version: Accepted Version

Article:

Bockwoldt, M., Houry, D., Niere, M. et al. (2019) Identification of evolutionary and kinetic drivers of NAD-dependent signaling. *Proceedings of the National Academy of Sciences*, 116 (32). pp. 15957-15966. ISSN: 0027-8424

<https://doi.org/10.1073/pnas.1902346116>

© 2019 The Authors. This is an author-produced version of a paper subsequently published in *Proceedings of the National Academy of Sciences*. Uploaded in accordance with the publisher's self-archiving policy.

Reuse

Items deposited in White Rose Research Online are protected by copyright, with all rights reserved unless indicated otherwise. They may be downloaded and/or printed for private study, or other acts as permitted by national copyright laws. The publisher or other rights holders may allow further reproduction and re-use of the full text version. This is indicated by the licence information on the White Rose Research Online record for the item.

Takedown

If you consider content in White Rose Research Online to be in breach of UK law, please notify us by emailing eprints@whiterose.ac.uk including the URL of the record and the reason for the withdrawal request.

Identification of evolutionary and kinetic drivers of NAD-dependent signalling

Mathias Bockwoldt¹, Dorothee Houry², Marc Niere², Toni Gossmann³, Ines Reinartz⁴, Alexander Schug⁵, Mathias Ziegler², Ines Heiland¹

¹University of Tromsø - The Arctic University of Norway, ²University of Bergen, ³University of Sheffield, ⁴Karlsruhe Institute of Technology, ⁵Jülich Research Centre (HZ)

Submitted to Proceedings of the National Academy of Sciences of the United States of America

NAD provides an important link between metabolism and signal transduction and has emerged as central hub between bioenergetics and all major cellular events. NAD-dependent signalling, e.g. by sirtuins and PARPs, consumes considerable amounts of NAD. To maintain physiological functions, NAD consumption and biosynthesis need to be carefully balanced. Using extensive phylogenetic analyses, mathematical modelling of NAD metabolism and experimental verification, we show that the diversification of NAD-dependent signalling in vertebrates depended on three critical evolutionary events: i) the transition of NAD biosynthesis to exclusive usage of nicotinamide phosphoribosyltransferase (NamPT); ii) the occurrence of nicotinamide N-methyltransferase (NNMT), which diverts nicotinamide (Nam) from recycling into NAD, preventing Nam accumulation and inhibition of NAD-dependent signalling reactions and iii) structural adaptation of NamPT, providing an unusually high affinity towards Nam, necessary to maintain NAD levels. Our results reveal an unexpected co-evolution and kinetic interplay between NNMT and NamPT that enables extensive NAD signalling. This has implications for therapeutic strategies of NAD supplementation and the use of NNMT or NamPT inhibitors in disease treatment.

NAD-dependent signalling | NAD biosynthesis | nicotinamide N-methyltransferase (NNMT) | nicotinamide phosphoribosyltransferase (NamPT) | phylogenetic pathway analysis; pathway evolution

Introduction

NAD metabolism has received increasing attention, as a number of pathological states including neurodegeneration (1), diabetes (2, 3), obesity (4-7), heart diseases (8, 9), muscle dystrophy (10), renal dysfunction (11) and different types of cancer (12-14) have been associated with changes in this complex network. It has been established that a gradual decline in NAD during ageing is one of the major driving forces of these age-related pathologies (15-18). In addition, NAD metabolism has been identified to be a key regulator for axonal integrity (19-21). It is therefore not surprising that NAD metabolism has emerged as promising pharmacological target for disease treatment (22-25). However, to fully exploit the therapeutic potential of NAD metabolism, the dynamic and functional interplay between the individual NAD pathway components need to be established.

NAD represents one of the most critical links between cellular signal transduction and energy metabolism. Even though it is best known as cofactor for a multitude of redox-reactions, NAD is involved in a number of signalling processes that consume NAD by cleaving NAD⁺ to nicotinamide (Nam) and ADP-ribose (14). These NAD-dependent signalling reactions include poly- and mono-ADP-ribosylation (26, 27), sirtuin-mediated protein deacetylation (28), and the synthesis of calcium-mobilizing molecules such as cyclic ADP-ribose (29), and participate in the regulation of virtually all cellular activities. The enzymes involved in these processes are sensitive to the available NAD concentration. Therefore, NAD-dependent signalling can act as a transmitter of changes in cellular energy homeostasis, for example, to regulate gene expression or metabolic activity (30).

The significance of NAD-dependent signalling for NAD homeostasis has long been underestimated. It has now become clear that inhibition of NAD biosynthesis leads to a rapid decline of the cellular NAD concentration (13, 31). This observation documents that NAD-dependent signalling reactions consume substantial amounts of NAD. The resulting NAD turnover differs in a cell-type-specific manner. Measurements of cellular NAD half-life have revealed that it can be as short as 15 minutes (32). To maintain the NAD concentration at physiological levels, NAD biosynthesis needs to act at an equally rapid rate. Imbalances in NAD homeostasis have been associated with a number of different diseases. In this context, it is conceivable that several recent studies have demonstrated impressive health benefits of dietary supplementation with intermediates of NAD biosynthesis including, Nam (4), Nam mononucleotide (NMN) (16) and Nam riboside (NR) (2, 6, 17). Apparently, the exploitation of physiologically less active NAD biosynthetic routes, in addition to the use of Nam as precursor (Figure 1), results in increased NAD concentrations that stimulate beneficial NAD-dependent signalling processes, in particular, protein deacetylation by sirtuins (3, 33).

Owing to the continuous release of Nam through NAD-consuming signalling reactions, NAD salvage using Nam as precursor is the most important NAD synthesis pathway. There are two principal pathways that recycle Nam. Vertebrates use a direct two-step pathway starting with the conversion of Nam into the mononucleotide NMN catalysed by Nam phosphoribosyltransferase (NamPT) using phosphoribosyl pyrophosphate

Significance

NAD is best known as essential cofactor of biochemical reactions. In addition, it is involved in the regulation of virtually all major cellular events. These NAD-dependent regulatory functions are mediated by enzymes (e.g. sirtuins, PARPs, ADP-ribose cyclases) that cleave the molecule to liberate nicotinamide (Nam). We show that diversification of NAD-dependent signaling in Deuterostomia was accompanied by an optimization of NAD biosynthesis to ensure efficient high affinity recycling of Nam into NAD through Nam-phosphoribosyltransferase (NamPT). In addition, a Nam-methyltransferase (NNMT) emerged which facilitates high NAD-dependent signaling turnover by preventing accumulation of inhibitory Nam. This unexpected kinetic interplay between NamPT and NNMT needs to be considered in therapeutic strategies targeting these enzymes.

Reserved for Publication Footnotes

137
138
139
140
141
142
143
144
145
146
147
148
149
150
151
152
153
154
155
156
157
158
159
160
161
162
163
164
165
166
167
168
169
170
171
172
173
174
175
176
177
178
179
180
181
182
183
184
185
186
187
188
189
190
191
192
193
194
195
196
197
198
199
200
201
202
203
204

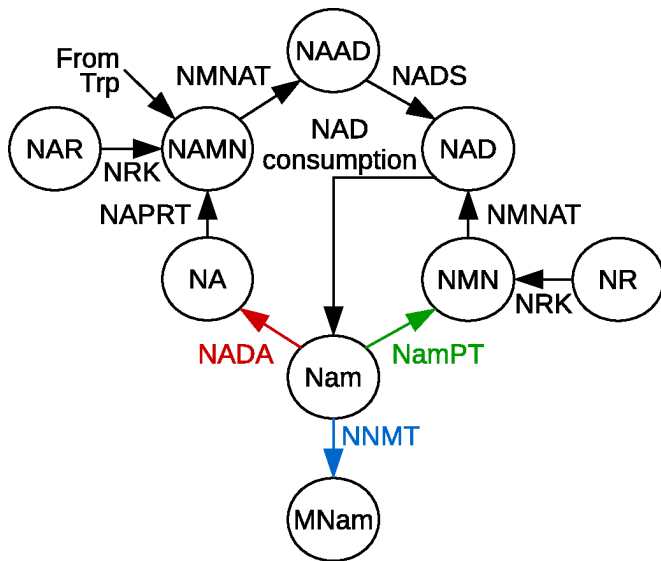


Fig. 1. Schematic overview of NAD biosynthesis pathways. NAD can be synthesised from tryptophan (Trp), nicotinamide (Nam), nicotinic acid (NA) and the corresponding ribosides NR and NAR. Nam is the main precursor in humans and also the product of NAD-consuming signalling reactions by enzymes such as sirtuins (NAD-dependent deacetylases) or PARPs (poly-ADP-ribose polymerases). For the recycling of Nam, two different pathways exist. The pathway found in yeast, plants, and many bacteria starts with the deamidation of Nam by Nam deamidase (NADA). Further biosynthesis via the Preiss-Handler pathway, which also exists in vertebrates, requires three subsequent enzymatic steps catalysed by Nicotinic acid phosphoribosyltransferase (NAPRT), Nicotinic acid/Nicotinamide mononucleotide adenyltransferase (NAMNAT) and NAD synthase (NADS). In vertebrates, Nam is directly converted to nicotinamide mononucleotide (NMN) by Nam phosphoribosyltransferase (NamPT). The Nam N-methyltransferase (NNMT) degrades Nam to methyl-Nam (MNam), which, in mammals, is excreted with the urine. The colour code for the three different enzymes utilizing Nam is used in subsequent figures to denote the presence of these enzymes in different organisms.

(PRPP) as co-substrate. At least in mammals, a nearly complete recycling of Nam by NamPT is achieved by an extraordinarily high substrate affinity to Nam, the K_M being in the low nanomolar range (34). This appears to be mediated by an ATP-dependent phosphorylation of a histidine residue in the catalytic core (35). Despite the importance of its salvage, Nam can also be marked for excretion by methylation. This reaction is catalysed by Nam N-methyltransferase (NNMT). The presence of this enzyme in vertebrates (36) is among the most enigmatic and counterintuitive features of NAD metabolism. While NamPT is seemingly optimised to recycle even the faintest amounts of Nam back into NAD synthesis, NNMT seems to have no metabolic function other than to remove Nam from NAD metabolism. However, since NNMT uses the general methylation source S-adenosylmethionine, it has been suggested that Nam methylation may act as a metabolic methylation sink (37).

In most prokaryotes as well as in plants and fungi, another pathway consisting of four reactions starting with the deamidation of Nam to nicotinic acid (NA) by the Nam deamidase (NADA) is used. (Figure 1). The three enzymes that act downstream of NADA belong to the Preiss-Handler pathway that also exists in vertebrates. In this pathway NA is converted into the corresponding mononucleotide (NAMN), in a reaction performed by the NA-specific phosphoribosyltransferase NAPRT. The conversion of both mononucleotides, NMN and NAMN, into their corresponding dinucleotides, NAD and NAAD, is catalysed by the Nam/NA adenyltransferases (NMNATs) that are essential in all organisms (38). The recycling pathway via NA finally requires re-amidation of NAAD by NAD synthase. This final reaction

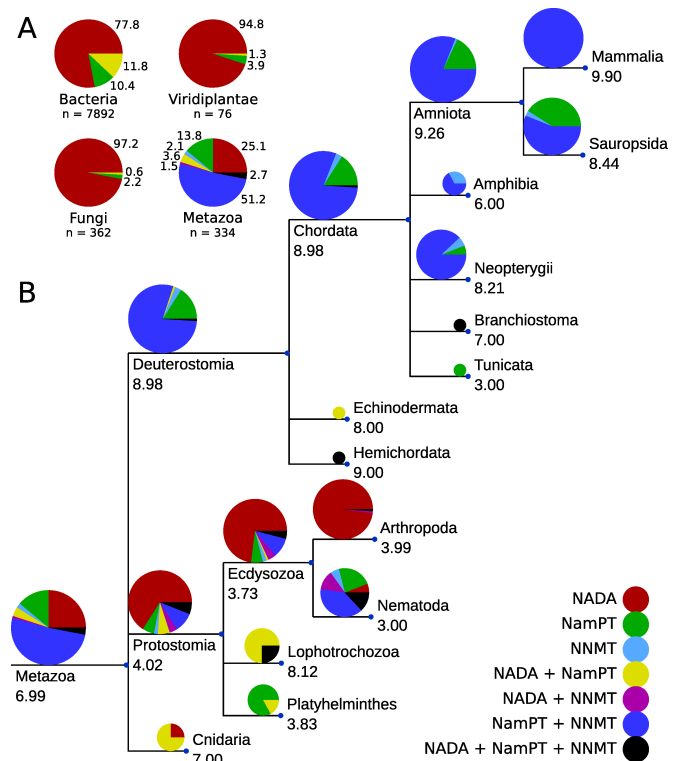


Fig. 2. Phylogenetic distribution of NADA, NNMT, and NamPT and their relation to the number of NAD consumers. A) Distribution of NADA, NNMT, and NamPT in selected clades. NADA is dominant in bacteria, fungi, and plants (Viridiplantae), whereas NamPT together with NNMT is dominant in Metazoa. Numbers at the pie charts show the percentage of species per clade, which possess the respective enzyme combination indicated by the colour code explained in the lower right of the figure (n = number of species per clade included in the analysis). B) Common tree of selected clades within Metazoa, including 334 species. The pie charts indicate the distribution of species within the respective clade that encode the enzyme combination indicated by the different colours. The size of the pie charts is proportional to the logarithm of the number of species analysed in the particular clade. The numbers below the clade names indicate the average number of NAD-consuming enzyme families found in all species of that clade. The branch length is arbitrary. A detailed analysis of birds is provided in S1 Appendix Figure S1 and the template sequences used for the analysis are listed in S1 Appendix Table S1.

includes an enzyme adenylation step that consumes ATP. Therefore, the Nam recycling by NADA appears to be energetically less efficient than the recycling pathway starting with NamPT.

We and others have shown earlier that the two NAD biosynthesis pathways starting from Nam (Figure 1) coexist in some eukaryotes (36, 39), as well as in some bacterial species (40). Why these pathways coexist in some organisms and over a very long evolutionary time frame and why NADA nevertheless disappeared in vertebrates, is not known. Whether the occurrence of NNMT may have contributed to these evolutionary processes has also remained unexplored.

In the present study, we performed a comprehensive phylogenetic analysis of the NAD pathways using 793 eukaryotic and 7892 prokaryotic genomes. This large scale analysis revealed that there has been an evolutionary transition resulting in the coexistence of NamPT and NNMT in Deuterostomia, while the deamidation pathway, which is dominant in bacteria, became superfluous. Importantly, this selection for NamPT and NNMT was accompanied by a marked increase in the number of NAD-consuming signalling enzymes. Mathematical modelling of the pathway revealed an unexpected positive kinetic role of NNMT for NAD-consuming signalling fluxes, through prevention of ac-

273
274
275
276
277
278
279
280
281
282
283
284
285
286
287
288
289
290
291
292
293
294
295
296
297
298
299
300
301
302
303
304
305
306
307
308
309
310
311
312
313
314
315
316
317
318
319
320
321
322
323
324
325
326
327
328
329
330
331
332
333
334
335
336
337
338
339
340

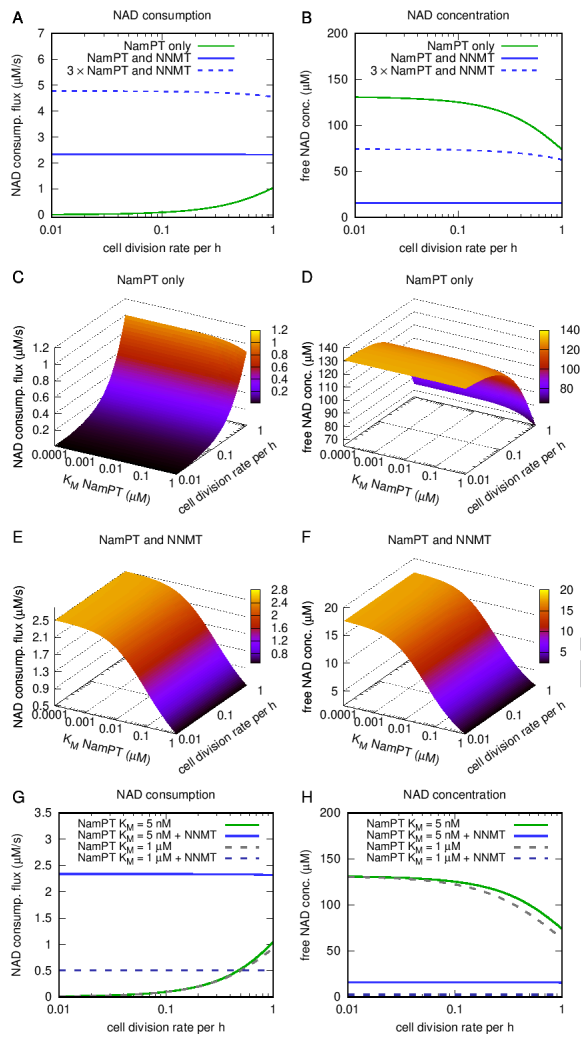


Fig. 3. NNMT enables high NAD consumption flux and is a potential driver of NamPT affinity increase. A dynamic model of NAD biosynthesis and consumption (for details, see Methods and Materials and SI Appendix Table S3) was used to simulate **A)** steady state NAD consumption flux and **B)** NAD concentration. Except for the results shown as dashed line in **A** and **B**, the enzyme amounts were kept constant for all simulations shown. In the presence of NNMT (blue curves), steady state NAD consumption rates are higher despite reduced NAD concentrations. Increasing the amount of NamPT in the simulation threefold (dotted blue curves) partially compensates for the decreased NAD concentration caused by Nam degradation through NNMT. The potential effect of different affinities of NamPT for Nam (inversely proportional to the Michaelis-Menten constant, K_M) on the steady state NAD consumption flux and NAD concentration was simulated at different cell division rates. In the absence of NNMT, the affinity of NamPT has little influence on **C)** NAD consumption and **D)** NAD concentration, but both are strongly influenced by cell division rates. **E** and **F)** in the presence of NNMT, increasing affinity of NamPT enables increasing NAD consumption flux and NAD concentration. The presence of NNMT makes both NAD consumption flux and NAD concentration almost independent of cell division rates. **G** and **H)** calculated NAD consumption fluxes and free NAD concentrations, respectively, are shown for the assumption of high affinity of NamPT ($K_M = 5$ nM, as found in the human enzyme) and low affinity (1 μ M, dashed lines). Comparing the situation with and without NNMT reveals that, at low substrate affinity of NamPT and high cell division rates, NNMT no longer enables higher NAD consumption rates compared to NamPT alone (green curves and dashed grey curves).

cumulation of Nam, the product of NAD-dependent signalling reactions. In addition, our model predicts that NNMT likely exerted an evolutionary pressure on NamPT to develop a high

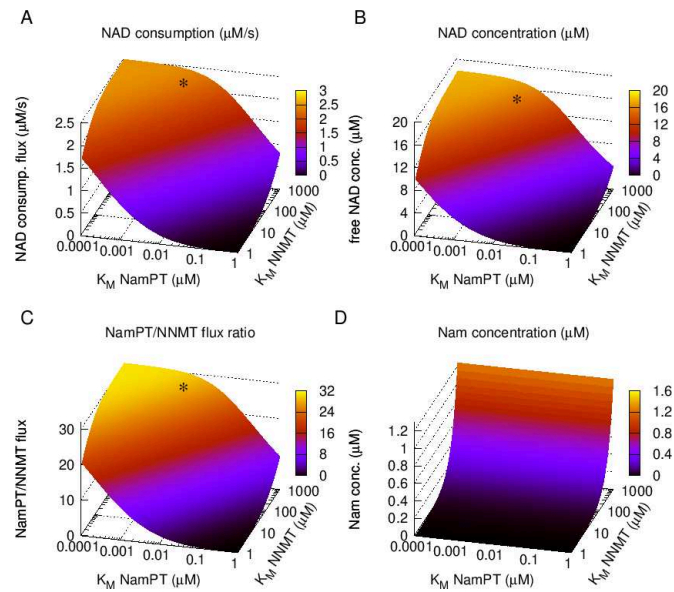


Fig. 4. Evolutionary optimality of the substrate affinities of human NNMT and NamPT. We simulated the impact of changes in the substrate affinities of both NamPT and NNMT on **A)** NAD consumption rates, **B)** free NAD concentration, **C)** NamPT/NNMT flux ratio and **D)** Nam concentration. With increasing affinity of NamPT (decreasing K_M), but decreasing affinity of NNMT (increasing K_M) NAD consumption rates and free NAD concentrations as well as the ratio between NamPT and NNMT flux are augmented. The affinities reported for human enzymes (indicated by a black asterisk) appear to be in the optimal range according to our simulations. The steady state concentration of Nam is largely independent of the substrate affinity of NamPT, but strongly dependent on the affinity of NNMT.

affinity towards its substrate Nam. Indeed, we identified a short sequence insertion in NamPT, which first occurs in Deuterostomia and appears to modulate the affinity of NamPT. Simulating resource competition, we furthermore show that the presence of high affinity NamPT together with NNMT makes the NADA-dependent pathway obsolete, providing a rationale for the evolutionary transition of the pathway in Metazoa.

Taken together, our analyses suggest that the coexistence of NamPT and NNMT has been a prerequisite to enable the evolutionary development of versatile NAD-dependent signalling mechanisms present in vertebrates.

Results

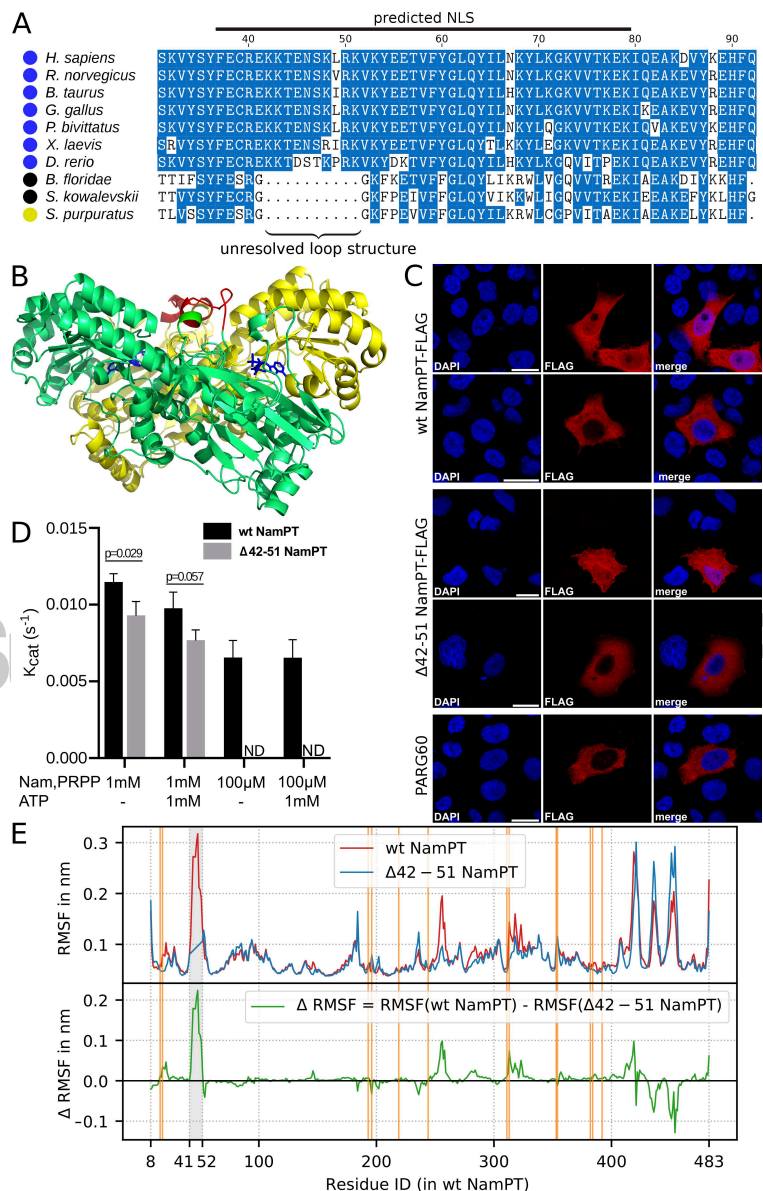
Paradoxical evolutionary correlation between NAD-dependent signalling and precursor metabolism

To understand the functional roles and potential interplay between the three known enzymes that use Nam as substrate (NamPT, NADA and NNMT, Figure 1), we conducted a comprehensive analysis of the phylogenetic distribution of these three enzymes. As shown in Figure 2A, bacteria, fungi, and plants predominantly possess NADA and only a very limited number of species harbour NamPT. In contrast, most Metazoa lost NADA, and rather possess NamPT together with NNMT. NADA and NamPT, the two enzymes that initiate the two different NAD salvage pathways, show a scattered distribution in bacteria. Co-occurrence of these enzymes is rather rare, and has occasionally been found in bacteria (40) and some marine invertebrates (36).

NNMT seems to have arisen *de novo* or diverged rapidly in the most recent common ancestor of Ecdysozoa and Lophotrochozoa (Figure 2B). We were unable to find any indication for the presence of NNMT in fungi or plants (Blastp e-value cutoff 0.1). Interestingly, NA can be methylated to trigonelline in plants and bacteria (41), but the corresponding enzyme has no homology to NNMT or any other enzyme in Metazoa. Nematodes are the

341
342
343
344
345
346
347
348
349
350
351
352
353
354
355
356
357
358
359
360
361
362
363
364
365
366
367
368
369
370
371
372
373
374
375
376
377
378
379
380
381
382
383
384
385
386
387
388
389
390
391
392
393
394
395
396
397
398
399
400
401
402
403
404
405
406
407
408

409
410
411
412
413
414
415
416
417
418
419
420
421
422
423
424
425
426
427
428
429
430
431
432
433
434
435
436
437
438
439
440
441
442
443
444
445
446
447
448
449
450
451
452
453
454
455
456
457
458
459
460
461
462
463
464
465
466
467
468
469
470
471
472
473
474
475
476



477
478
479
480
481
482
483
484
485
486
487
488
489
490
491
492
493
494
495
496
497
498
499
500
501
502
503
504
505
506
507
508
509
510
511
512
513
514
515
516
517
518
519
520
521
522
523
524
525
526
527
528
529
530
531
532
533
534
535
536
537
538
539
540
541
542
543
544

Fig. 5. The function of the structurally unresolved loop of NamPT. **A**) Multiple sequence alignment of NamPT revealed a sequence insertion in the N-terminal region of this enzyme in most Deuterostomia that possess NamPT and NNMT. The relevant sequence section is shown for selected organisms. A more comprehensive alignment can be found in SI Appendix Figure S2. Coloured circles indicate the enzymes present in the respective species; blue: NamPT and NNMT; black: NamPT, NADA and NNMT; yellow: NamPT and NADA. **B**) The structure visualisation of human NamPT is based on a structure prediction by SWISS-MODEL (74, 75) using the model 2H3D of the human NamPT as template (65). The region corresponding to amino acids 42-51 (shown in red) in the human enzyme is not resolved in any of the currently available crystal structures of NamPT and thus appears to be a flexible loop at the surface of the NamPT dimer. **C**) Confocal laser scan micrographs of HeLaS3 cells expressing C-terminally FLAG-tagged wildtype (wt) and mutant Δ42-51 NamPT lacking the unresolved loop. Both proteins showed a heterogeneous nuclear-cytosolic localisation. Nuclei were stained with DAPI. The C-terminally FLAG-tagged human poly-ADP-ribose glycohydrolase isoform PARG60 was used as a control for exclusive cytosolic localization. (scale bars = 20 μm) **D**) Measurement of NamPT (wildtype and Δ42-51 mutant) enzymatic activity in the presence of 1 mM or 100 μM substrate (Nam and PRPP) with or without 1mM ATP (ND, no detection of the reaction product, NMN). The p-value was calculated using non-parametric one-tailed Mann-Whitney test. The His-tagged proteins were expressed in *E. coli* and purified as described in Methods and Materials (see also SI Appendix Figure S4). **E**) Molecular dynamics simulations were performed for wildtype (red) and Δ42-51 NamPT (blue). Root mean square fluctuations (RMSF) for every residue of chain A are shown (top). The difference RMSF for every residue is shown in the lower panel (green). For better comparison the residue IDs for Δ42-51 NamPT are aligned to accord with the wildtype structure and the average RMSF of residues 42 and 51 displayed in the blue curve between these residues. For the RMSF calculation, the first 100 ns of the simulation are omitted to allow equilibration. In addition, root mean square deviation (RMSD) values between different published structures of human NamPT structures were calculated and presented in SI Appendix Table S4 and Figure S5. The orange lines indicate the position of residues involved in substrate binding, according to Burgos et al. 2009 (35).

only organisms in which we observed a concomitant presence of NADA and NNMT. In Deuterostomia, the only large clade that possesses only NamPT and seems to have lost NNMT are Sauropsida, and among them especially birds. The reason why

about half of the sequenced bird genomes do not seem to harbour *NNMT* remains unclear. The distribution of *NNMT* in birds is quite scattered (SI Appendix Figure S1). It is possible that detection of *NNMT* in some bird genomes failed because of their

545
546
547
548
549
550
551
552
553
554
555
556
557
558
559
560
561
562
563
564
565
566
567
568
569
570
571
572
573
574
575
576
577
578
579
580
581
582
583
584
585
586
587
588
589
590
591
592
593
594
595
596
597
598
599
600
601
602
603
604
605
606
607
608
609
610
611
612

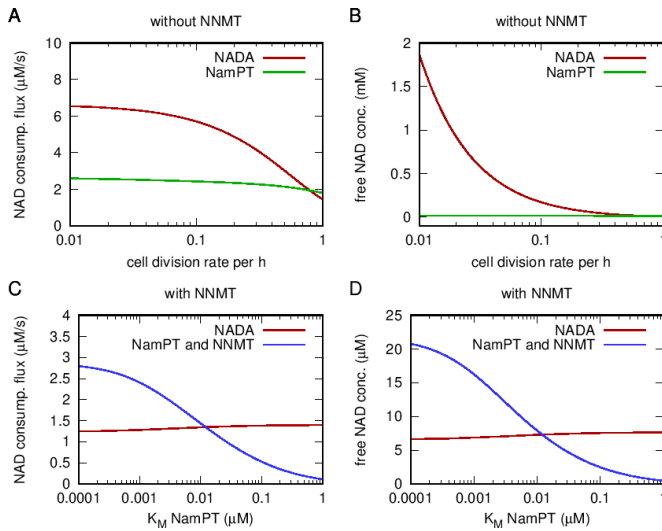


Fig. 6. NNMT provides a competitive advantage and makes NADA obsolete in vertebrates. To simulate competition for common resources, a two-compartment model was created (see Methods and Materials and SI Appendix Table S3). In this model one compartment contained NADA, but no NamPT and the other compartment contained NamPT either with or without NNMT, but no NADA. NADA and NamPT were simulated to be present at equal amounts. **A)** In the absence of NNMT, the compartment containing NADA has a higher NAD consumption rate, and **B)** a considerably higher steady state NAD concentration. **C)** In the presence of NNMT, however, both NAD consumption and **D)** NAD concentration are lower in the NADA compartment. This effect is dependent on a high affinity of NamPT for Nam.

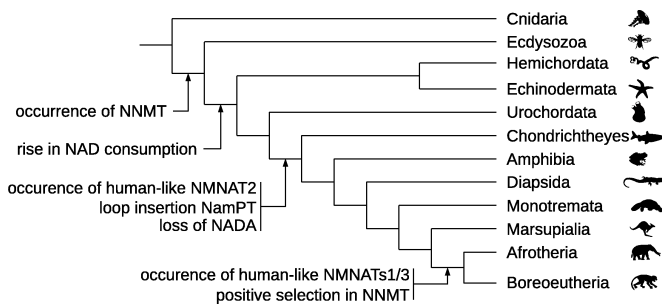


Fig. 7. Schematic representation of evolutionary events in the NAD biosynthesis pathway The scheme illustrates major evolutionary events in Metazoa detected in our phylogenetic analyses of NAD metabolism. The time of occurrence of human like NMNAT1 and 3 has been reported previously(61), and identified that human-like NMNAT2 most likely originated in the last common ancestor (LCA) of vertebrates, while human-like NMNAT1/3 can be traced back to the LCA of Placentalia (SI Appendix Figure S9). To test whether the rise of human like NMNAT1/3s was associated with an event of rapid sequence diversification in NNMT we conducted a test of positive selection specific to the branch leading to the LCA of Placentalia using a coding DNA substitution rate ratio model. Indeed, we obtain a strong signature of positive selection for NNMT in the tested branch and can pinpoint residue 171 as being significantly associated with the signature of positive selection (SI Appendix Figures S7 and S8). Specific events in the evolution of NMNATs coincide with those of NamPT or NNMT indicating a co-evolution of functions beyond those identified in the present study. The tree is a schematic representation of selected taxa and is based on information provided by the Tree of life Web Project (76).

high GC content (42) or because of difficulties in assembling very small chromosomes commonly found in birds. The absence of *NNMT* might, alternatively, be related to the differences in the excretion systems. In mammals, the product of *NNMT*, methyl-Nam, is excreted with the urine. There are few metazoan species for which we could not find *NamPT* or *NADA*, while *NNMT* was

detected. We assume that this is due to incomplete genomes in the database, as these species are scarce and their distribution appears to be randomly scattered.

In addition to the phylogenetic distribution of the two *Nam* salvage enzymes *NADA* and *NamPT*, we analysed the phylogenetic diversity of enzymes catalysing NAD-dependent signalling reactions. To do so, we used the previously established classification into ten different families of NAD-consuming signalling enzymes (36), including *PARP1-3*, *PARP4*, *PARP6/8*, *PARP7/9-15*, *PARP16*, sirtuins, tankyrases, *ADPR-cyclases*, *mono-ADP-ribosyltransferases* and *t-RNA-phosphotransferases*. The detailed list of templates used for the phylogenetic analyses can be found in SI Appendix Table S1. The numbers shown in Figure 2B denote the average number of NAD-dependent signalling enzyme families found in each clade (for a detailed distribution see SI Appendix Table S2). With the exception of *Cnidaria* and *Lophotrochozoa*, we noted an average of three to four families in protostomes, whereas most deuterostome species have, on average, more than eight families with an increasing diversification of enzymes within some of these families, especially *PARPs* (43).

Taken together, we found that *NADA* is lost in vertebrates, but strongly preserved in most other organisms, despite the higher energetic requirement of this pathway. Moreover, the transition to having both *NamPT* and *NNMT* coincides with a considerable diversification of NAD-dependent signalling. This observation seems counter-intuitive, as one would expect that increased NAD-dependent signalling should be compensated by an increased efficiency of substrate (*Nam*) utilization for NAD biosynthesis. Since *NNMT* removes *Nam* from recycling into NAD, it is not obvious how this enzyme could contribute to higher NAD turnover.

Functional properties of NamPT and NNMT have evolved to maximise NAD-dependent signalling

To resolve this apparent contradiction, we turned to modelling approaches permitting to simulate the behaviour of the complex NAD metabolic network under different conditions. We built a dynamic model of NAD metabolism based on ordinary differential equations using previously reported kinetic data (for details, see Methods and Materials and SI Appendix Table S3).

Given the rather limited information about species-specific expression levels of enzymes, we first assumed equal expression of all enzymes, thereby enabling an initial comparison of metabolic features in rather different organisms. Moreover, due to the lack of specific kinetic data from most organisms, we mainly relied on kinetic constants found for human or yeast enzymes. Wherever possible, we included substrate affinities and known product inhibitions as well as inhibition by downstream metabolites, such as the inhibition of *NamPT* by NAD (34). Finally, the models assumed that cell growth and consecutive cell divisions are a major driving force for NAD biosynthesis, besides NAD-consuming reactions.

First, we addressed the observed phylogenetic correlation between the transition to the co-occurrence of *NamPT* and *NNMT* and the increase in the number of NAD-consuming enzymes. We calculated steady state NAD concentrations and NAD consumption fluxes by simulating NAD biosynthesis via *NamPT* in the presence or absence of *NNMT* (Figure 3 A and B). Due to the very low turnover number of *NamPT* (~0.01/s), we used 40-fold higher *NamPT* levels compared to the other enzymes to achieve free NAD concentrations in the range reported in the literature (44). NAD concentrations can be further increased with higher *NamPT* levels (see SI Appendix Figure S3A and B). Since *NamPT* limits the flux, changing *NMNAT* levels had no effect under the conditions tested (SI Appendix Figure S3 A and B).

Surprisingly, our simulations predict that the presence of *NNMT* enables higher rather than lower NAD consumption fluxes (Figure 3A), although it diminishes the steady state concen-

681 tration of NAD (Figure 3B). The decline in NAD concentration
682 can be compensated by a higher expression of NamPT, which
683 also further increases NAD consumption flux (dashed lines in
684 Figure 3A and B). These results indicate a stimulatory role for
685 NNMT solely on the basis of the enzyme kinetics, without having
686 to invoke any regulatory mechanism (such as signalling events).
687 It turns out that these results can be explained on the basis of
688 the kinetic parameters of NamPT and NAD-consuming enzymes
689 such as Sirtuin 1 (Sirt1). Most NAD-consuming enzymes are
690 inhibited by their product, Nam. Thus, the presence of NNMT
691 enables higher NAD consumption fluxes, by removing excess
692 Nam from the system (SI Appendix Figure S3D and E). At the
693 same time, a high substrate affinity of NamPT ensures the
694 maintenance of a sufficiently high NAD concentration, although
695 the concentration is, as expected, lower than in the system without
696 NNMT. To verify that the release of Nam inhibition is indeed
697 responsible for the increase in NAD consumption flux, we simu-
698 lated the network with varying K_i values for the NAD consuming
699 reaction. As can be inferred from SI Appendix Figures S3E and
700 F, increasing the K_i for Nam in a system without NNMT mimics
701 the situation when NNMT is included. In contrast, changing the
702 K_i of NamPT for NAD has no effect. That is, decreased NamPT
703 inhibition by lowered NAD concentrations does not cause the
704 flux increase observed in the presence of NNMT. However, if the
705 NAD concentration is strongly reduced, due to high expression
706 of NNMT, the NAD consumption declines again (SI Appendix
707 Figure S3C and D).

708 Kinetic parameters of NamPT were previously reported for
709 the human enzyme (34) as well as for some bacterial enzymes
710 (45), the latter having a much lower substrate affinity for Nam.
711 We thus simulated the potential effect of NamPT affinity (K_M)
712 on NAD steady state concentration and NAD consumption flux.
713 In the absence of NNMT, a variation of the substrate affinity of
714 NamPT for Nam is predicted to have very little effect on steady
715 state NAD concentration and NAD consumption flux (Figure 3C
716 and D). In the presence of NNMT, however, NAD consumption
717 flux and NAD concentration would rise with increasing affinity of
718 NamPT (Figure 3E and F).

719 Remarkably, NAD concentration and consumption flux are
720 both considerably affected by cell division rates in a system
721 without NNMT. Our simulations predict a trade-off between
722 sustainable NAD concentration and consumption flux, in the
723 absence of NNMT. In the presence of NNMT, however, NAD
724 consumption rates and concentrations are almost independent of
725 cell division rates. These observations point to a role of NNMT
726 for NAD homeostasis at varying cell division and consumption
727 rates.

728 Given that a lower affinity of NamPT has been described for
729 the bacterial enzyme (45) where NNMT is not present, we were
730 wondering if the advantage provided by NNMT is dependent on
731 a high affinity of NamPT. In Figures 3G and H we show the
732 direct comparison of simulations assuming different affinities of
733 NamPT, in the presence or absence of NNMT. Interestingly, a low
734 affinity that is in the range of the affinity of NADA for Nam and
735 far above those measured for bacterial NamPTs, leads to higher
736 NAD consumption flux in the presence of NNMT, but only, when
737 cell division rates are low (Figure 3G). However, if the affinity of
738 NamPT is high enough ($K_M \ll 1 \mu\text{M}$), consumption rates are
739 always higher with NNMT than without. The NAD concentration
740 is, as would be assumed, always lower with NNMT (Figure 3H).

741 To understand the interplay and competition for Nam be-
742 tween NamPT and NNMT, we conducted simulations in which
743 we scanned a wide range of possible substrate affinities for both
744 enzymes. As shown in Figure 4, these simulations indicate that
745 both NAD consumption flux and NAD concentration would be
746 minimal in case of a low substrate affinity of NamPT and high
747 affinity of NNMT. Conversely, increasing the affinity of NamPT

748 increases NAD consumption, NAD concentration and the flux
749 ratio between NamPT and NNMT reaching a plateau when the
750 substrate affinity of NNMT is sufficiently low. Remarkably, as
751 indicated by the asterisks in Figure 4A, B and C the reported
752 substrate affinities for human NamPT and NNMT (K_M of 5nM
753 and 400 μM , respectively) are within the predicted optimal range,
754 where further adjustment would lead to little or no increase
755 of NAD consumption flux, NAD concentration or NamPT to
756 NNMT flux ratio.

757 *Sequence variance acquired in metazoan NamPT enhances* 758 *substrate affinity*

759 Given the kinetic interdependence of NNMT and NamPT
760 revealed above, it seemed possible that NNMT exerted an evo-
761 lutionary pressure on the development of NamPT. In this case,
762 one would expect to observe adaptations that are reflected in
763 the NamPT protein sequence arising in conjunction with the
764 occurrence of NNMT. To explore this, we created a multiple
765 sequence alignment of NamPT protein sequences from Metazoa.
766 An alignment of selected sequences is shown in Figure 5A, a more
767 comprehensive multiple sequence alignment containing a larger
768 number of species can be found in SI Appendix Figure S2. We
769 found an insert of ten amino acids in most Deuterostomia that
770 possess only NamPT and NNMT (indicated by the blue circle,
771 Figure 5A). This insert corresponds to positions 42 to 51 in the
772 human enzyme and overlaps with a predicted weak nuclear local-
773 isation signal (NLS). The NLS prediction is lost when the insert is
774 removed. The ten amino acid insert has so far not been resolved in
775 any of the available crystal structures obtained for NamPT. When
776 modelling this stretch into the known homodimeric structure, the
777 predicted loop, depicted in red in Figure 5B, is connected to one
778 of the β -sheets involved in substrate binding (35). Intriguingly, the
779 loops of the two subunits are in close proximity.

780 From these observations, we derived two possible hypotheses
781 regarding the role of the loop in NamPT function. The first
782 hypothesis is that the presence of the loop could affect the subcel-
783 lular localisation of NamPT, as it is overlapping with a predicted
784 NLS. To test this hypothesis, we created a mutant NamPT lacking
785 the loop and recombinantly expressed FLAG-tagged wildtype
786 and mutant NamPT in HeLa S3 cells. Immunofluorescence imag-
787 ing showed a mixed cytosolic/nuclear localisation for both the
788 wildtype and the mutant NamPT (Figure 5C). Thus, deletion of
789 the loop did not compromise nuclear localisation.

790 The second hypothesis is based on our model simulations
791 that predict that the presence of NNMT might have exerted
792 evolutionary pressure on NamPT kinetics and that therefore the
793 sequence insertion might have an effect on substrate binding of
794 NamPT. To analyse this possibility, we expressed and purified
795 the wildtype and the mutant enzyme, which lacks the stretch
796 of amino acids 42-51, in *E. coli*, N-terminally fused to a 6xHis-
797 tag. The size exclusion chromatography profile showed that both
798 wildtype and mutant protein were expressed as dimers (see SI
799 Appendix Figure S4C), indicating that the mutant protein was
800 likely folded correctly. The enzymatic activity was assessed by
801 measuring NMN formation. Upon incubation with the NamPT
802 inhibitor FK866 (31) for 30 minutes, neither wildtype nor mutant
803 NamPT did synthesize NMN, suggesting that binding of FK866 is
804 not affected by the mutation (SI Appendix Figure S4D). Using
805 100 μM Nam and PRPP as substrates, the wildtype showed a
806 turnover rate of $0.0065 \pm 0.0010 \text{ s}^{-1}$ and $0.0077 \pm 0.0006 \text{ s}^{-1}$ without
807 and with ATP, respectively, while the mutant did not have any
808 detectable activity (Figure 5D). With 1 mM of both substrates, the
809 turnover rate of the wildtype enzyme increased to 0.0115 ± 0.0005
810 s^{-1} and $0.0098 \pm 0.0010 \text{ s}^{-1}$ without and with ATP, respectively.
811 Under these conditions, the turnover rate of the mutant enzyme
812 was $0.0093 \pm 0.0008 \text{ s}^{-1}$ and $0.0077 \pm 0.0006 \text{ s}^{-1}$ without and
813 with ATP, respectively. When keeping both PRPP and ATP constant
814 at 1 mM, the wildtype enzyme reaches its maximal rate in the low
815
816

micromolar range of Nam concentrations (SI Appendix Figure S4E). Under these conditions, activity of the mutant is detectable only at submillimolar Nam concentrations and still rises between 0.5 and 1 mM (SI Appendix Figure S4E) indicating a far lower affinity towards Nam compared to the wildtype. The decrease in activity with ATP at high concentrations of substrates has been observed earlier (34) and has been attributed to the competitive binding of ATP and PRPP (35). Overall, our observations suggest that human NamPT lacking the amino acid stretch 42-51 is catalytically active, retains its dimeric state and sensitivity to FK866. However, it has a lower activity and affinity to Nam. These observations lend support to the conclusion that the acquisition of this loop in the NamPT of higher vertebrates has led to an increased affinity to Nam, as predicted by our metabolic modelling approach.

To see whether we can find a molecular explanation for the reduced affinity of the mutant enzyme, we analysed different available protein structures of NamPT and tested whether the loop insertion could potentially lead to dynamic structural rearrangements. To this end we applied homology modelling (Figure 5B) and molecular dynamics simulations for structures with and without the loop insertion (Figure 5E). We did not observe substantial structural rearrangements and the molecular dynamics simulations showed only limited structural changes upon loop deletion. Rather, we observed a mostly structurally stable catalytic core. This might be based on the fact that all available protein structures of NamPT differ very little even at the catalytic site (between 0.33Å and 0.95Å see SI Appendix Table S4). Some residues close to the catalytic site showed slightly elevated mobilities in the wildtype structure. However, these elevated mobilities were dominated by rare events during the simulation time of 1µs. They therefore do not appear as a robust change of structural dynamics upon loop insertion.

NNMT made NADA obsolete in vertebrates

Finally, we wished to understand whether NADA may have been lost in vertebrates due to kinetic constraints. As shifts in evolutionary selection pressure may result from competition for resources, we built a two-compartment model, based on the pathway model described above. One compartment contains NADA, while the other one contains either NamPT alone or together with NNMT. Both compartments share a limited Nam source (for model details see SI Appendix Table S3). Without NNMT, the compartment containing NADA shows a higher NAD consumption rate (Figure 6A), and is able to maintain much higher NAD concentrations especially at low cell division rates (Figure 6B). At high cell division rates, steady state concentrations and NAD-consumption rates in both compartments are similar. As bacteria often have relatively high growth rates and a low number of NAD consuming enzymes, this might explain why, at least in some bacteria, both systems may co-exist.

In the presence of NNMT, the NamPT compartment has both higher NAD consumption rates and higher steady state NAD concentrations than the compartment containing NADA (Figure 6C and 6D). This is, however, dependent on the affinity of NamPT for Nam. If the substrate affinity of NamPT is too low, the NADA compartment is able to maintain higher NAD concentrations and consumption flux. As shown in SI Appendix Figure S6, expression of NADA in addition to NNMT and NamPT provides a slight advantage over NADA alone, as long as NamPT has a low affinity. Taken together, the results suggest that the NADA pathway might have helped in the transition to high affinity NamPT, potentially explaining its co-occurrence with NamPT and NNMT in some invertebrates. Eventually, NADA became obsolete upon emergence of a high affinity NamPT. This, in turn, might have been induced by the appearance of NNMT.

Discussion

The present study has revealed fundamental new insights into the evolution and dynamic interplay of the enzymes in NAD metabolism. Our results show that the occurrence of NNMT enabled the enormous diversification of NAD-consuming signalling enzymes in Deuterostomia. NNMT promotes the removal of excessive Nam produced in the signalling reactions. This is necessary to overcome Nam inhibition of the corresponding enzymes. To enable both high NAD turnover and continuous salvage of Nam into NAD, the kinetic parameters of both human NamPT and NNMT have attained values that are in the optimal range predicted through our simulations (Figure 4). Our analyses have identified a stretch of 10 amino acids in the structure of NamPT which contributes to the unusually high substrate affinity of this enzyme in higher vertebrates. While it remains unclear why lower organisms and plants use primarily the Nam salvage pathway through NADA, our analyses demonstrate that the combination of NamPT and NNMT outcompetes this alternative when high turnover of NAD is required for signalling processes. Consequently, NADA has been lost in vertebrates.

The positive effect of NNMT on NAD-consumption flux, especially on sirtuins, is in line with a lifespan extension observed in worms overexpressing NNMT (46). The effect of NNMT overexpression or silencing has been controversially discussed and is presumably tissue and context specific (37). In this regard, it should be noted that, although we predict an overall positive effect of NNMT on NAD consumption rates, excessive expression of NNMT can lead to adverse effects (SI Appendix Figure S3C). Moreover, our analyses predict that the presence of NNMT generally lowers the Nam concentration and reduces cellular NAD concentrations. This effect can, however, be counterbalanced by increased NamPT expression (47, 48). The moderate effects of NNMT expression changes on NAD concentrations (SI Appendix Figure S3D) might explain why some experimental results reported in the literature seem inconsistent. For example, a considerable decrease of liver NAD levels has been reported upon NNMT overexpression (49), while no changes in NAD concentrations could be detected in other studies (5, 50).

It has been shown that M_{Nam} excretion is mostly proportional to Nam uptake (51), supporting our findings that NNMT contributes to NAD-pathway homeostasis. As shown in several recent studies, this homeostatic control by NNMT can be circumvented by supplying NR (2, 52-54) which is not a substrate of NNMT. At the cellular level, NNMT is presumably mainly advantageous, when high NAD-consumption rates are required for tissue function, or even more likely, might be important to prevent spatio-temporal accumulation of Nam within cells due to temporally increased NAD-consumption, e.g. PARP activation through DNA-damage.

The main healthy tissues expressing NNMT are the liver and adipose tissues, while no or only little expression of NNMT is observed in most other organs (55). Increased NNMT expression has been found in several types of cancer (56, 57), and might serve to remove Nam produced by increased NAD-dependent signalling. To maintain high NAD concentrations in the tumours, a concomitant increase of NamPT expression is required, which has indeed been described for some cancers (47, 48). It is worth noticing that NNMT is only advantageous as long as NamPT affinity and activity are sufficiently high. This suggests that certain types of cancers, which express NNMT at a high level, could potentially be more susceptible to inhibitors of NamPT. Several of such inhibitors are currently tested in clinical studies (23, 58). Based on our analyses, it might be reasonable to test patients for NNMT expression in the tumour tissue. Non-NNMT expressing tumours might respond less to competitive NamPT inhibitors, because deficient Nam degradation in those cancer cells would

953 potentially lead to an accumulation of Nam that could outcom-
954 pete the inhibitor.

955 Neither the scattered distribution of NamPT and NADA that
956 is especially pronounced in bacteria (40), nor the loss of NADA
957 in the ancestor of vertebrates has been understood earlier. Our
958 combined phylogenetic-modelling analysis provides a potential
959 explanation for both observations. Using simulated competition
960 between two compartments that share the same limited source of
961 Nam, we show that the compartment that contains NamPT and
962 NNMT can maintain a higher steady state NAD concentration
963 and NAD consumption rate than the compartment containing
964 NADA (Figure 6). This is, however, only the case, if NamPT's
965 substrate affinity is sufficiently high. The dominant enzyme com-
966 bination found in vertebrates, a high-affinity NamPT along with
967 NNMT, thus seems to provide a competitive advantage when high
968 NAD turnover rates are needed. This is not necessarily the case
969 in organisms that use Nam recycling through NADA

970 In our analyses, we did not consider the potential effects
971 of most co-substrates of the investigated pathway. These co-
972 substrates include targets of the NAD-consuming enzymes, such
973 as acylated proteins for sirtuins, or phosphoribosyl pyrophos-
974 phate (PRPP) and ATP required for NMN synthesis by NamPT.
975 However, we did perform an analysis of the effect of concentra-
976 tion changes in the methyl donor S-adenosyl methionine (SAM).
977 Its precursor methionine has been shown to potentially limit
978 the effect of NNMT (57). As shown in SI Appendix Figures
979 S3G and H SAM can have both positive and negative effects
980 on the NAD consumption flux, depending on the SAM concen-
981 tration range. The effects observed in the physiological SAM
982 concentration range (59) are, however, much smaller than those
983 observed for expression changes in NNMT or NamPT (SI Ap-
984 pendix Figure S3C and A respectively). Nevertheless, changes in
985 methionine metabolism, might under some conditions influence
986 cellular NAD concentration and NAD consumption rates. As
987 NNMT in turn consumes SAM, NNMT might not only provide
988 a kinetic advantage for NAD metabolism, but is likely to have a
989 role in regulating other cellular processes through its impact on
990 SAM availability (37). For example, it has been shown that the
991 product MNam can induce the expression of sirtuins (46, 50, 60).
992 However, the underlying mechanisms are still unknown.

993 In conclusion, we have comprehensively analysed the func-
994 tional co-evolution of several enzymes of the NAD pathway. The
995 appearance of NNMT apparently initiated and drove complex al-
996 terations of the pathway such as an increase and diversification
997 of NAD-dependent signalling, paralleled by an increase in NamPT
998 substrate affinity. Remarkably, when analysing the possibility of
999 co-evolutionary developments within the NAD pathway, we also
1000 noted that the loss of NADA and the loop insertion in NamPT
1001 co-occurred with the appearance of a human-like NMNAT2
1002 (schematic overview see Figure 7, details SI Appendix Figure S7-
1003 S9). Moreover, the occurrence of human-like NMNATs 1 and 3
1004 and thus the further compartmentalisation of NAD metabolism
1005 (61) coincided with a site-specific positive selection event in
1006 NNMT (see SI Appendix Figure S7 and S8). This might point
1007 to a role of NNMT in NAD pathway compartmentalisation in
1008 addition to spatio-temporal regulation of the pathway in general.

1009 Methods and Materials

1010 Phylogenetic Analysis

1011 Functionally verified sequences of NNMT, NADA, NamPT,
1012 and NAD-consuming enzymes were used as sequence templates
1013 for a Blastp analysis against the NCBI non-redundant protein
1014 sequence database. For a list of template sequences see SI Ap-
1015 pendix Table S1. Blastp parameters were set to yield maximum
1016 20 000 target sequences, using the BLOSUM62 matrix with a
1017 word size of 6 and gap opening and extension costs of 11 and
1018 1, respectively. Low-complexity filtering was disabled. To prevent
1019 cross-hits, a matrix was created in which the lowest e-values were

1020 given at which Blast yielded the same result for each query protein
1021 pair. With help of the matrix, the e-value cut-off was set to 1e-
1022 30 for all enzymes. To further prevent false positives, a minimal
1023 length limit was set based on a histogram of the hit lengths
1024 found for each query protein, excluding peaks much lower than
1025 the total protein length. Length limits are given in SI Appendix
1026 Table S1. In addition, obvious sequence contaminations were
1027 removed by manual inspection of the results. The taxonomy IDs
1028 of the species for each enzyme was derived from the acces-
1029 sion2taxonomy database provided by NCBI. Scripts for creat-
1030 ing, analysing, and visualising the phylogenetic tree were written
1031 in Python 3.5, using the ETE3 toolkit (62) and are accessible
1032 through the following GitHub repository [https://github.com/M-](https://github.com/MolecularBioinformatics/Phylogenetic-analysis)
1033 [olecularBioinformatics/Phylogenetic-analysis](https://github.com/MolecularBioinformatics/Phylogenetic-analysis).

1034 Dynamic modelling

1035 Kinetic parameters (substrate affinity (K_M) and turnover rates
1036 (k_{cat}), substrate and product inhibitions) were retrieved from the
1037 enzyme database BRENDA and additionally evaluated by check-
1038 ing the original literature especially with respect to measurement
1039 conditions. Parameter values from mammalian species were used
1040 if available. For enzymes not present in mammals, values from
1041 yeast were integrated. The full list of kinetic parameters including
1042 reference to original literature can be found in SI Appendix Table
1043 S3. For NMNAT, the previously developed rate law for substrate
1044 competition was used (63). Otherwise, Henri-Michaelis-Menten
1045 kinetics were applied for all reactions except the import and efflux
1046 of Nam, which were simulated using constant flux and mass action
1047 kinetics, respectively. Steady state calculation and parameter scan
1048 tasks provided by COPASI 4.25 (64) were used for all simulations.
1049 The model files are accessible through the Biomodels database
1050 accession no. MODEL1905220001 and MODEL1905220002. Re-
1051 lated figures were generated using Gnuplot 5.0.

1052 Generation of expression vectors encoding wildtype and mutant 1053 human NamPT

1054 For eukaryotic expression with a C-terminal FLAG-epitope,
1055 the open reading frame (ORF) encoding human NamPT was
1056 inserted into pFLAG-CMV-5a (Merck - Sigma Aldrich) via
1057 EcoRI/BamHI sites. Using a PCR approach, this vector provided
1058 the basis for the generation of a plasmid encoding a NamPT de-
1059 lection mutant lacking amino acid residues 42-51 (Δ 42-51 NamPT).
1060 For prokaryotic expression with an N-terminal 6xHis-tag, the
1061 wildtype and mutant ORFs were inserted into pQE-30 (Qiagen)
1062 via BamHI and PstI-sites. All cloned sequences were verified by
1063 DNA sequence analysis.

1064 Transient transfection, immunocytochemistry, and confocal 1065 laser scanning microscopy

1066 HeLa S3 cells cultivated in Ham's F12 medium supple-
1067 mented with 10% (v/v) FCS, 2 mM L-glutamine, and peni-
1068 cillin/streptomycin, were seeded on cover slips in a 24 well plate.
1069 After one day, cells were transfected using Effectene transfection
1070 reagent (Qiagen) according to the manufacturer's recommen-
1071 dations. Cells were fixed with 4% paraformaldehyde in PBS 24
1072 hours post transfection, permeabilised (0.5% (v/v) Triton X-100
1073 in PBS) and blocked for one hour with complete culture medium.
1074 After overnight incubation with primary FLAG-antibody (mouse
1075 M2, Sigma-Aldrich) diluted 1:2500 in complete medium, cells
1076 were washed and incubated for one hour with secondary Alex-
1077 aFluor 594-conjugated goat anti mouse antibody (ThermoFisher,
1078 Invitrogen) diluted 1:1000 in complete culture medium. Nuclei
1079 were stained with DAPI and the cells were washed. The cover
1080 slips were mounted onto microscope slides using ProLong Gold
1081 (ThermoFisher, Invitrogen). Confocal laser scanning microscopy
1082 of cells was performed at the Molecular Imaging Center at the
1083 Department of Biomedicine (University of Bergen), using a Leica
1084 TCS SP8 STED 3x microscope equipped with a 100x oil immer-
1085 sion objective (numerical aperture 1.4).

1086 NamPT expression

E. coli BL21-CodonPlus (DE3)-RIL (Agilent) were transformed with pQE-30 NamPT WT or pQE-30 Δ 42-51 NamPT along with pREP4 (Qiagen) encoding the lac repressor. Bacterial cells were grown at 37°C in 1 L of Luria-Bertani broth supplemented with 100 μ g/mL ampicillin, 50 μ g/mL kanamycin and 32 μ g/mL chloramphenicol. Protein expression was induced with 0.2 mM isopropyl- β -D-thiogalactoside at 0.4~0.6 OD₆₀₀, and cells were subsequently grown overnight at 18 °C.

Purification of NamPT

The cells were harvested by centrifugation and resuspended in lysis buffer (20 mM Tris-HCl pH 8.0, 500 mM NaCl, 4 mM dithiothreitol (DTT), 1 mg/ml lysozyme, 1X Complete EDTA-free protease inhibitor cocktail (Roche)). After sonication, the lysate was centrifuged at 13,000 g for 30 min. The supernatant was incubated with 2 ml of Nickel-NTA resin (Qiagen). Non-specific protein binding was removed with washing buffer (20 mM Tris-HCl pH 8.0, 500 mM NaCl, 1 mM DTT, 20 mM imidazole). The protein was eluted with 2.5 ml of elution buffer (20 mM Tris-HCl pH 8.0, 500 mM NaCl, 1 mM DTT, 300 mM imidazole).

The eluted protein was immediately subjected to size exclusion chromatography (SEC) using an ÄKTA pure system (GE Healthcare) equipped with a HiLoad 16/60 Superdex 200 pg column (GE Healthcare). The chromatography was performed at a flow rate of 1 ml/min with SEC buffer (20 mM Tris-HCl pH 8.0, 500 mM NaCl). Fractions containing the recombinant protein were pooled and used for enzymatic assays. The purity and size of the protein were assessed by SDS-PAGE.

Enzymatic Assay

In a final volume of 1.2 ml reaction buffer (20 mM Tris-HCl pH 8.0, 500 mM NaCl, 6 mM MgCl₂, 0.03% (w/v) BSA), 2 μ M of enzyme were incubated with 5-phospho-D-ribose 1-diphosphate (PRPP) and Nam (100 μ M or 1 mM both). The reaction was incubated at 30 °C for 10 min and stopped by adding 100 μ M of FK866. Subsequently, the samples were frozen in liquid nitrogen. The amount of NMN produced was analysed using NMR spectroscopy. To do so the samples were dried with an Eppendorf Vacufuge Concentrator, and then resuspended in 200 μ l of NMR solvent containing 5% (v/v) deuterated H₂O and 1 mM 4,4-dimethyl-4-silapentane-1-sulfonate (DSS). 1D ¹H NMR spectra were acquired on a 850 MHz Ascend Bruker spectrometer equipped with 5 mm TCI triple-resonance CryoProbe and a pulse field gradient along the z-axis. The spectra were acquired with the zgpg30 pulse sequence, allowing water suppression using excitation sculpting with gradients and perfect echo. The temperature was kept constant at 300 K. Data were acquired with 2000 scans, 1 s relaxation delay, 1.6 s acquisition time, and contained 65,000 data points with a spectral width of 14 ppm. The spectra phase and baseline were automatically and manually corrected using TopSpin 3.5 software (Bruker Biospin). Quantification of nicotinamide mononucleotide (NMN) was done by the integration of the peak at 9.52 ppm and DSS used as an internal

standard. The raw measurement data are accessible using doi: 10.15490/fairdomhub.1.datafile.2942.1

All experiments were conducted at the Norwegian NMR Platform, NNP (grant 226244/F50).

Molecular dynamics simulations

All-atom molecular dynamics simulations were performed with explicit solvent for wildtype and mutant Δ 42-51 NamPT (PDB Code: 2H3D (65)). AMBER99SB-ILDN force field (66) was used with the TIP3P water model (67) in GROMACS 5.1.2 (68). The structures were simulated each in a box of water with distance between the solute and the box set to 0.2 nm at a temperature of 300 K for a total time of 1 μ s. A time step of 2 fs and the stochastic dynamics integrator were used. For the evaluation of the root mean square fluctuations (RMSF) the first 100 ns of the simulations were omitted.

Identification of human-like NMNATs and test of positive selection in NNMNTs

For the identification of human-like NMNATs we clustered the retrieved sequences using BALi-Phy (69) (SI Appendix Figure S9). Human-like NMNATs 1, 2, and 3 were identified based on the isoform-specific targeting and interaction domains described in (61).

We conducted a test of positive selection for orthologs of human NNMT from 60 vertebrate species. We obtained coding sequences for all species and aligned the respective protein-translated sequences using MUSCLE (70) and prepared codon-based alignments for further processing with PAL2NAL (71). We used codeml from the PAML package (72) to conduct a branch-site model A test of positive selection. The species names and the underlying tree topology for the codeml runs is depicted in SI Appendix Figure S8B. As a null model we assumed neutrality (e.g. diversifying site class with dN/dS = ω = 1) which then was compared to a model with positive selection (dN/dS = ω > 1). Significance between the two models is assessed using a likelihood ratio test assuming that twice the likelihood difference is χ^2 distributed. The critical value is 3.84 at the 5% level. Additionally, we identify codons with a site-specific signal of positive selection using a Bayes Empirical Bayes (BEB) analysis with a probability > 0.9 (73).

Acknowledgements

We thank the Norwegian Research Council for funding (grant no. 250395/F20). We furthermore thank for the computation time provided through UNINETT Sigma2 – the National Infrastructure for High Performance Computing and Data Storage in Norway. MZ was supported by a grant from the Norwegian Cancer Society (grant no. 673238). IR and AS received support by the Helmholtz Association Initiative and Networking Fund under project number ZT-I-0003. TIG is supported by a Leverhulme Early Career Fellowship (Grant ECF-2015-453) and a NERC grant (NE/N013832/1). The authors thank Heiko Stark for advice with respect to taxonomic classifications. *Author contribution* IH and MZ conceived the study. MB and TG performed the phylogenetic analysis, IH performed the mathematical modelling, DH and MN performed the experiments, IR performed the MD analyses guided by AS. MZ and IH supervised and guided the investigations. All authors analysed data and contributed to the manuscript preparation. *Declaration of interests* The authors declare no competing interest.

105(5):481-491.

1. Ljungberg MC, et al. (2012) CREB-activity and nmnat2 transcription are down-regulated prior to neurodegeneration, while NMNAT2 over-expression is neuroprotective, in a mouse model of human tauopathy. *Hum Mol Genet* 21(2):251-267.
2. Trammell SA, et al. (2016) Nicotinamide Riboside Opposes Type 2 Diabetes and Neuropathy in Mice. *Sci Rep* 6:26933.
3. Yoshino J, Mills KF, Yoon MJ, & Imai S (2011) Nicotinamide mononucleotide, a key NAD(+) intermediate, treats the pathophysiology of diet- and age-induced diabetes in mice. *Cell Metab* 14(4):528-536.
4. Mitchell SJ, et al. (2018) Nicotinamide Improves Aspects of Healthspan, but Not Lifespan, in Mice. *Cell Metab* 27(3):667-676 e664.
5. Kraus D, et al. (2014) Nicotinamide N-methyltransferase knockdown protects against diet-induced obesity. *Nature* 508(7495):258-262.
6. Canto C, et al. (2012) The NAD(+) precursor nicotinamide riboside enhances oxidative metabolism and protects against high-fat diet-induced obesity. *Cell Metab* 15(6):838-847.
7. Kann T, et al. (2018) A small molecule inhibitor of Nicotinamide N-methyltransferase for the treatment of metabolic disorders. *Sci Rep* 8(1):3660.
8. Hsu CP, Oka S, Shao D, Hariharan N, & Sadoshima J (2009) Nicotinamide phosphoribosyltransferase regulates cell survival through NAD+ synthesis in cardiac myocytes. *Circ Res* 105(5):481-491.
9. Diguett N, et al. (2018) Nicotinamide Riboside Preserves Cardiac Function in a Mouse Model of Dilated Cardiomyopathy. *Circulation* 137(21):2256-2273.
10. Ryu D, et al. (2016) NAD+ repletion improves muscle function in muscular dystrophy and counters global PARylation. *Sci Transl Med* 8(361):361ra139.
11. Poyan Mehr A, et al. (2018) De novo NAD(+) biosynthetic impairment in acute kidney injury in humans. *Nat Med* 24(9):1351-1359.
12. Chiarugi A, Dölle C, Felici R, & Ziegler M (2012) The NAD metabolome – A key determinant of cancer cell biology. *Nature Reviews Cancer* 12(11):741–752.
13. Buonvicino D, et al. (2018) Identification of the Nicotinamide Salvage Pathway as a New Toxication Route for Antimetabolites. *Cell Chemical Biology* 25(4):471–482.e477.
14. Verdin E (2015) NAD+ in aging, metabolism, and neurodegeneration. *Science* 350(6265).
15. Chini CCS, Tarrago MG, & Chini EN (2017) NAD and the aging process: Role in life, death and everything in between. *Mol Cell Endocrinol* 455:62-74.
16. Mills KF, et al. (2016) Long-Term Administration of Nicotinamide Mononucleotide Mitigates Age-Associated Physiological Decline in Mice. *Cell Metab* 24(6):795-806.

1225	17. Zhang H, et al. (2016) NAD(+) repletion improves mitochondrial and stem cell function and enhances life span in mice. <i>Science</i> 352(6292):1436-1443.	1293
1226	18. Imai SI & Guarente L (2016) It takes two to tango: NAD(+) and sirtuins in aging/longevity control. <i>NPJ Aging Mech Dis</i> 2:16017.	1294
1227	19. Araki T, Sasaki Y, & Milbrandt J (2004) Increased nuclear NAD biosynthesis and SIRT1 activation prevent axonal degeneration. <i>Science</i> 305(5686):1010-1013.	1295
1228	20. Beirowski B, et al. (2009) Non-nuclear Wld(S) determines its neuroprotective efficacy for axons and synapses in vivo. <i>J Neurosci</i> 29(3):653-668.	1296
1229	21. Di Stefano M, et al. (2017) NMN Deamidase Delays Wallerian Degeneration and Rescues Axonal Defects Caused by NMNAT2 Deficiency In Vivo. <i>Curr Biol</i> 27(6):784-794.	1297
1230	22. Yoshino J, Baur JA, & Imai SI (2018) NAD(+) Intermediates: The Biology and Therapeutic Potential of NMN and NR. <i>Cell Metab</i> 27(3):513-528.	1298
1231	23. Espindola-Netto JM, et al. (2017) Preclinical efficacy of the novel competitive NAMPT inhibitor STF-118804 in pancreatic cancer. <i>Oncotarget</i> 8(49):85054-85067.	1299
1232	24. Rajman L, Chwalek K, & Sinclair DA (2018) Therapeutic Potential of NAD-Boosting Molecules: The In Vivo Evidence. <i>Cell Metab</i> 27(3):529-547.	1300
1233	25. Sinclair DA & Guarente L (2014) Small-molecule allosteric activators of sirtuins. <i>Annu Rev Pharmacol Toxicol</i> 54:363-380.	1301
1234	26. Gupte R, Liu Z, & Kraus WL (2017) PARPs and ADP-ribosylation: recent advances linking molecular functions to biological outcomes. <i>Genes Dev</i> 31(2):101-126.	1302
1235	27. Bütepage M, Eckerl L, Verheugd P, & Lüscher B (2015) Intracellular Mono-ADP-Ribosylation in Signaling and Disease. <i>Cells</i> 4(4):569-595.	1303
1236	28. Osborne B, Bentley NL, Montgomery MK, & Turner N (2016) The role of mitochondrial sirtuins in health and disease. <i>Free Radical Biology and Medicine</i> 100:164-174.	1304
1237	29. Lee HC (2012) Cyclic ADP-ribose and nicotinic acid adenine dinucleotide phosphate (NAADP) as messengers for calcium mobilization. <i>Journal of Biological Chemistry</i> 287(38):31633-31640.	1305
1238	30. Koch-Nolte F, Haag F, Guse AH, Lund F, & Ziegler M (2009) Emerging roles of NAD+ and its metabolites in cell signaling. <i>Science Signaling</i> 2(57):mr1.	1306
1239	31. Hasmann M & Schemainda I (2003) FK866, a highly specific noncompetitive inhibitor of nicotinamide phosphoribosyltransferase, represents a novel mechanism for induction of tumor cell apoptosis. <i>Cancer Res</i> 63(21):7436-7442.	1307
1240	32. Liu L, et al. (2018) Quantitative Analysis of NAD Synthesis-Breakdown Fluxes. <i>Cell Metabolism</i> 27(5):1067-1080.e1065.	1308
1241	33. North BJ & Verdin E (2004) Sirtuins: Sir2-related NAD-dependent protein deacetylases. <i>Genome Biology</i> 5(5):224.	1309
1242	34. Burgos ES & Schramm VL (2008) Weak coupling of ATP hydrolysis to the chemical equilibrium of human nicotinamide phosphoribosyltransferase. <i>Biochemistry</i> 47(42):11086-11096.	1310
1243	35. Burgos ES, Ho M-C, Almo SC, & Schramm VL (2009) A phosphoenzyme mimic, overlapping catalytic sites and reaction coordinate motion for human NAMPT. <i>Proceedings of the National Academy of Sciences</i> 106(33):13748-13753.	1311
1244	36. Gossmann TI, et al. (2012) NAD+ biosynthesis and salvage – a phylogenetic perspective. <i>The FEBS Journal</i> 279(18):3355-3363.	1312
1245	37. Pissios P (2017) Nicotinamide N-Methyltransferase: More Than a Vitamin B3 Clearance Enzyme. <i>Trends in Endocrinology and Metabolism</i> 28(5):340-353.	1313
1246	38. de Figueiredo LF, Gossmann TI, Ziegler M, & Schuster S (2011) Pathway analysis of NAD+ metabolism. <i>Biochemical Journal</i> 439(2):341-348.	1314
1247	39. Carneiro J, et al. (2013) The Evolutionary Portrait of Metazoan NAD Salvage. <i>PLoS ONE</i> 8(5).	1315
1248	40. Gazzaniga F, Stebbins R, Chang SZ, McPeck MA, & Brenner C (2009) Microbial NAD metabolism: lessons from comparative genomics. <i>Microbiology and Molecular Biology Reviews</i> 73(3):529-541.	1316
1249	41. Perchat N, et al. (2018) Elucidation of the trigonelline degradation pathway reveals previously undescribed enzymes and metabolites. <i>Proc Natl Acad Sci U S A</i> 115(19):E4358-E4367.	1317
1250	42. Hron T, Pajer P, Pačes J, Bartůněk P, & Elleder D (2015) Hidden genes in birds. <i>Genome Biology</i> 16(1):4-7.	1318
1251	43. Gossmann TI & Ziegler M (2014) Sequence divergence and diversity suggests ongoing functional diversification of vertebrate NAD metabolism. <i>DNA Repair</i> 23:39-48.	1319
1252	44. Cambronne XA, et al. (2016) Biosensor reveals multiple sources for mitochondrial NAD(+). <i>Science</i> 352(6292):1474-1477.	1320
1253	45. Sorci L & Blaby Ia (2010) Genomics-driven reconstruction of Acinetobacter NAD metabolism: Insights for antibacterial target selection. <i>Journal of Biological Chemistry</i> 285(50):39490-39499.	1321
1254	46. Schmeisser K, et al. (2013) Role of sirtuins in lifespan regulation is linked to methylation of nicotinamide. <i>Nature Chemical Biology</i> 9(11):693-700.	1322
1255	47. Bi TQ, et al. (2011) Overexpression of Nampt in gastric cancer and chemopotentiating effects of the Nampt inhibitor FK866 in combination with fluorouracil. <i>Oncology Reports</i> 26(5):1251-1257.	1323
1256	48. Wang B, et al. (2011) NAMPT overexpression in prostate cancer and its contribution to tumor cell survival and stress response. <i>Oncogene</i> 30(8):907-921.	1324
1257	49. Komatsu M, et al. (2018) NNMT activation can contribute to the development of fatty liver disease by modulating the NAD(+) metabolism. <i>Sci Rep</i> 8(1):8637.	1325
1258	50. Hong S, et al. (2015) Nicotinamide N-methyltransferase regulates hepatic nutrient metabolism through Sirt1 protein stabilization. <i>Nature Medicine</i> 21(8):887-894.	1326
1259	51. Kang-Lee YA, et al. (1983) Metabolic effects of nicotinamide administration in rats. <i>J Nutr</i> 113(2):215-221.	1327
1260	52. Gong B, et al. (2013) Nicotinamide riboside restores cognition through an upregulation of proliferator-activated receptor-gamma coactivator 1alpha regulated beta-secretase 1 degradation and mitochondrial gene expression in Alzheimer's mouse models. <i>Neurobiol Aging</i> 34(6):1581-1588.	1328
1261	53. Liu HW, et al. (2018) Pharmacological bypass of NAD(+) salvage pathway protects neurons from chemotherapy-induced degeneration. <i>Proc Natl Acad Sci U S A</i> .	1329
1262	54. Martens CR, et al. (2018) Chronic nicotinamide riboside supplementation is well-tolerated and elevates NAD(+) in healthy middle-aged and older adults. <i>Nat Commun</i> 9(1):1286.	1330
1263	55. Aksoy S, Szumlanski CL, & Weinshilboum RM (1994) Human liver nicotinamide N-methyltransferase. cDNA cloning, expression, and biochemical characterization. <i>Journal of Biological Chemistry</i> 269(20):14835-14840.	1331
1264	56. Okamura A, et al. (1998) Increased hepatic nicotinamide N-methyltransferase activity as a marker of cancer cachexia in mice bearing colon 26 adenocarcinoma. <i>Japanese Journal of Cancer Research</i> 89(6):649-656.	1332
1265	57. Ulanovskaya OA, Zuhl AM, & Cravatt BF (2013) NNMT promotes epigenetic remodeling in cancer by creating a metabolic methylation sink. <i>Nature Chemical Biology</i> 9(5):300-306.	1333
1266	58. Xu T-Y, et al. (2015) Discovery and characterization of novel small-molecule inhibitors targeting nicotinamide phosphoribosyltransferase. <i>Scientific Reports</i> 5(1):10043.	1334
1267	59. Reed MC, Nijhout HF, Sparks R, & Ulrich CM (2004) A mathematical model of the methionine cycle. <i>J Theor Biol</i> 226(1):33-43.	1335
1268	60. Liu KY, et al. (2015) Nicotinamide N-methyltransferase increases complex I activity in SH-SY5Y cells via sirtuin 3. <i>Biochem Biophys Res Commun</i> 467(3):491-496.	1336
1269	61. Lau C, et al. (2010) Isoform-specific targeting and interaction domains in human nicotinamide mononucleotide adenylyltransferases. <i>J Biol Chem</i> 285(24):18868-18876.	1337
1270	62. Huerta-Cepas J, Serra F, & Bork P (2016) ETE 3: Reconstruction, Analysis, and Visualization of Phylogenomic Data. <i>Molecular Biology and Evolution</i> 33(6):1635-1638.	1338
1271	63. Schäuble S, Stavrum A-K, Puntervoll P, Schuster S, & Heiland I (2013) Effect of substrate competition in kinetic models of metabolic networks. <i>FEBS Letters</i> 587(17):2818-2824.	1339
1272	64. Hoops S, et al. (2006) COPASI – a COmplex PATHway Simulator. <i>Bioinformatics</i> 22(24):3067-3074.	1340
1273	65. Wang T, et al. (2006) Structure of Nampt/PBEF/visfatin, a mammalian NAD+ biosynthetic enzyme. <i>Nature Structural and Molecular Biology</i> 13(7):661-662.	1341
1274	66. Lindorff-Larsen K, et al. (2010) Improved side-chain torsion potentials for the Amber ff99SB protein force field. <i>Proteins</i> 78(8):1950-1958.	1342
1275	67. Jorgensen WL, Chandrasekhar J, Madura JD, Impey RW, & Klein ML (1983) Comparison of simple potential functions for simulating liquid water. <i>The Journal of Chemical Physics</i> 79(2):926-935.	1343
1276	68. Abraham MJ, et al. (2015) GROMACS: High performance molecular simulations through multi-level parallelism from laptops to supercomputers. <i>SoftwareX</i> 1-2:19-25.	1344
1277	69. Suchard MA & Redelings BD (2006) BALI-Phy: simultaneous Bayesian inference of alignment and phylogeny. <i>Bioinformatics</i> 22(16):2047-2048.	1345
1278	70. Edgar RC (2004) MUSCLE: a multiple sequence alignment method with reduced time and space complexity. <i>BMC Bioinformatics</i> 5:113.	1346
1279	71. Suyama M, Torrents D, & Bork P (2006) PAL2NAL: robust conversion of protein sequence alignments into the corresponding codon alignments. <i>Nucleic Acids Res</i> 34(Web Server issue):W609-612.	1347
1280	72. Yang Z (2007) PAML 4: phylogenetic analysis by maximum likelihood. <i>Mol Biol Evol</i> 24(8):1586-1591.	1348
1281	73. Yang Z, Wong WS, & Nielsen R (2005) Bayes empirical bayes inference of amino acid sites under positive selection. <i>Mol Biol Evol</i> 22(4):1107-1118.	1349
1282	74. Arnold K, Bordoli L, Kopp J, & Schwede T (2006) The SWISS-MODEL workspace: A web-based environment for protein structure homology modelling. <i>Bioinformatics</i> 22(2):195-201.	1350
1283	75. Biasini M, et al. (2014) SWISS-MODEL: Modelling protein tertiary and quaternary structure using evolutionary information. <i>Nucleic Acids Research</i> 42(W1):252-258.	1351
1284	76. Anonymus (2007) Tree of Life Web Project. eds Maddison DR & Schulz K-S.	1352
1285		1353
1286		1354
1287		1355
1288		1356
1289		1357
1290		1358
1291		1359
1292		1360